Degradation of ciprofloxacin using heterogeneous Fenton catalysts derived from natural pyrite and rice straw biochar

Fan Sang[a,1], Zhuo Yin[b,1], Wenjun Wang[c,1], Eydhah Almatrafi[d,1], Yuwen Wang[a], Beichen Zhao[a], Jilai Gong[a], Chengyun Zhou[a], Chen Zhang[a], Guangming Zeng[a,*], Biao Song[a,*]

[a] College of Environmental Science and Engineering and Key Laboratory of Environmental Biology and Pollution Control (Ministry of Education), Hunan University, Changsha 410082, PR China;

[b] Department of Urology, Second Xiangya Hospital, Central South University, Changsha 410011, PR China;

[c] School of Resources and Environment, Hunan University of Technology and Business, Changsha 410205, China

[d] Center of Research Excellence in Renewable Energy and Power Systems, Center of Excellence in Desalination Technology, Department of Mechanical Engineering, Faculty of Engineering-Rabigh, King Abdulaziz University, Jeddah 21589, Saudi Arabia.

* Corresponding authors at College of Environmental Science and Engineering, Hunan University, Changsha 410082, PR China.

Tel: +86 731 88822754; Fax: +86 731 88823701.

E-mail addresses: zgming@hnu.edu.cn (G. Zeng); songbiao@hnu.edu.cn (B. Song)

1 These authors contribute equally to this article.

Abstract

The increased use of antibiotics and the discharge of antibiotic wastewater have caused severe pollution, and there is an urgent need for innovative treatment technologies. In this study, a novel catalyst derived from two low-cost materials natural pyrite (FeS_2) and rice straw biochar (BC) for the heterogeneous Fenton degradation of ciprofloxacin (CIP) was prepared, namely natural pyrite modified rice straw biochar (FeS_2/BC). The catalyst was synthesized by grinding and calcination without adding any chemical reagents. The effects of catalyst dosage, pH value, hydrogen peroxide concentration, different anions and reusability on CIP degradation were investigated. Under the optimal conditions, the FeS_2/BC system can degrade 96.8% of CIP (30 mg/L) within 20 min, thereby realizing the rapid degradation of CIP. Except HCO_3^-, common anions in water including Cl^-, NO_3^- and SO_4^{2-} displayed no impact on the CIP degradation. Excellent degradation performance was owed to the synergy of attack by free radicals and adsorption. Hydroxyl radical(•OH), superoxide radical ($O_2^{\bullet-}$) and sulfate radical ($SO_4^{\bullet-}$) existed in the system at the same time and •OH was the dominant active species for degrading CIP. Both biochar and S(−II) promoted the conversion of Fe species. This work provides a novel heterogeneous Fenton catalyst from the resource utilization of solid waste, and realizes waste elimination and pollution reduction simultaneously, which has good scientific and practical value.

Keywords: Pyrite; Biochar; Fenton; Advanced oxidation; Wastewater treatment

1. Introduction

Alongside the growing evolution of biological and chemical technology, antibiotics are generally applied in therapy of diseases including human and nonhuman (Michael et al., 2013; Oberoi et al., 2019). Since most antibiotics cannot be fully and thoroughly metabolized in organisms, vast quantities of antibiotics are injected into the environment through wastewater discharge from breeding industry, pharmaceutical factory, and domestic activities (Chen et al., 2020a; Nguyen et al., 2020; Zhang et al., 2021). Ciprofloxacin (CIP) is a broadly used fluoroquinolone antibiotics, and besides it often occurs as the degradation product of another commonly used antibiotic enrofloxacin (He et al., 2022; Zhou et al., 2022). As the second-generation fluoroquinolone, ciprofloxacin has stable chemical structure and is difficult to biodegrade and transform in aqueous system. The conventional technology in wastewater treatment plants such as nitrification/denitrification has limited removal rate of ciprofloxacin (Van Doorslaer et al., 2014). The concentration of ciprofloxacin residual in aquatic environment, ranges from ng/L to mg/L, with a maximum of 31 mg/L. The residual ciprofloxacin causes severe pollution and ecological risk, such as inhibiting the normal activity of microorganisms in the original environment and leading to the continuous diffusion of antibiotic resistance (Girardi et al., 2011; Hanna et al., 2018). Therefore, removal of ciprofloxacin in the environment is particularly necessary and urgent.

Advanced oxidation processes (AOPs), which remove organic pollutants by

producing active free radicals, have been successfully used in wastewater treatment (Wang and Xu, 2012; Tian et al., 2020; Wang and Zhuan, 2020). Fenton process is a well-established AOP, which degrades contaminants through the oxidation of hydroxyl radicals (·OH) generated by the reaction between Fe^{2+} and H_2O_2. In view of the threshold of the traditional homogeneous Fenton processes, such as strict reaction conditions, the follow-up treatment of iron-containing sludge, and difficult recovery of catalysts (Li et al., 2019), the heterogeneous Fenton processes using solid catalyst instead of soluble divalent iron salts have attracted wide attention. Using solid catalyst can effectively achieve the catalyst recovery, reduce the iron sludge production and broaden the application range (Wang and Tang, 2021a; Wang and Tang, 2021b).

Biochar (BC) is a kind of carbon-rich material, which is obtained by pyrolysis of biomass (plant, animal or sludge) in oxygen-free or oxygen-limited environment (Khan et al., 2013; Dong et al., 2017; Zhou et al., 2020). With the advantages of environmentally friendly characteristic, low cost, good adsorption and stable structure, biochar is broadly used in dealing with wastewater (Premarathna et al., 2019; Pan et al., 2021; Song et al., 2022b), and has made achievements in the treatment of many pollutants such as antibiotics (Krasucka et al., 2021; Qin et al., 2022a; Qin et al., 2022b), pesticides (Varjani et al., 2019), dyes (Lyu et al., 2018) and heavy metals (Inyang et al., 2016). However, due to the shortcomings of the original biochar, such as limited specific surface area, weak catalytic activity and adsorption-dominant removal (Lyu et al., 2020; Yi et al., 2020), it usually needs to be modified before being used as

heterogeneous Fenton catalyst (Pan et al., 2021). For example, Deng et al. (2018) loaded nanometer zero-valent iron on corn straw biochar (nZVI/BC) and applied it for the removal of sulfamethazine by Fenton-like reaction, and the removal capacity of the nZVI/BC was nearly twice that of the original biochar. Park et al. (2018) prepared iron modified biochar by impregnating bagasse in ferrous sulfate solution and the catalyst was applied to remove Orange G from water by Fenton-like reaction, and the removal rate of Orange G could be maintained over 89.3% after four sequential uses. It can be found that the catalytic performance of biochar is greatly improved after combining with iron element.

Pyrite (FeS_2), one of the sulfides commonly found on earth, is a kind of mining waste with little value (Murphy and Strongin, 2009). In addition to its low price and wide sources, pyrite itself can reduce the Fe^{3+} produced by Fenton reaction as a reducing agent, and H^+ can be generated during the reaction to meet the low pH demand for Fenton processes (Bae et al., 2013; Zhu et al., 2020), which has gradually been accepted as an excellent heterogeneous Fenton material in the past few years. Zhang et al. (2014) used natural pyrite to degrade nitrobenzene in heterogeneous Fenton system and obtained a degradation rate of 80%, while that of classical Fenton system was only 30% in the same reaction time. Wang et al. (2021) applied natural pyrite to the heterogeneous Fenton treatment of dye wastewater, and achieved remarkable degradation effects on different dyes and mixed dyes.

However, to the best of our knowledge, there are few studies combining natural

pyrite with biochar as composite for heterogeneous Fenton reactions. In our assumption, when natural pyrite is loaded onto biochar, the latter can capture pollutants by virtue of its adsorption capacity and improved the weakness of poor adsorption capacity of natural pyrite, and pyrite can effectively catalyze the Fenton reaction to degrade pollutants. Furthermore, biochar can slow down Fe^{2+} releasing as a carrier and promote Fe^{3+} reduction as an electron donor (Diao et al., 2017; Qin et al., 2017; Wang et al., 2019), so as to achieve the cooperation of mutual advantages. As a big agricultural country, China produces about 2×10^8 t of waste straw every year. Turning these agricultural wastes into biochar realizes waste utilization and resource utilization, and rice straw biochar has been proven to be a material with good performance for removing antibiotics from water (Krasucka et al., 2021), therefore we decided to choose rice straw as the raw material for biochar. Selecting rice straw and natural pyrite as the raw materials of heterogeneous Fenton catalyst can realize waste elimination and pollutant degradation at the same time. The preparation process of the composite is planned to adopt the method of first grinding and then pyrolysis, and no additional chemical reagents are added during the preparation process to avoid waste. Hence, the aims of this paper are to: (1) synthesize natural pyrite modified rice straw biochar (FeS_2/BC) catalyst; (2) explore the performance of the Fenton system catalyzed by FeS_2/BC for degradation of CIP and the influence of reaction conditions on the degradation efficiency; and (3) elucidate the degradation mechanisms involved in the Fenton system catalyzed by FeS_2/BC.

2. Materials and methods

2.1. Materials

The natural pyrite (1–3 mm) was obtained from a mining area in Hengyang City, Hunan Province of China. Ciprofloxacin (CIP, $C_{17}H_{18}FN_3O_3$, purity>99.0%), tert-butanol (TBA), hydrogen peroxide (H_2O_2, 30%) and other reagents used were at least analytical grade. Ultra-pure water was used throughout the experiment.

2.2. Synthesis and characterization of FeS_2/BC catalyst

Rice straw was pyrolyzed at 500 ℃, the preparation method was consistent with our previous work (Song et al., 2022a), and the biochar product was ground and sieved through a 100-mesh sifter. Natural pyrite was pretreated the same as biochar for subsequent experiments. The synthesis steps of the FeS_2/BC were as follows: Firstly, BC and FeS_2 were fully mixed by grinding in an agate mortar together. According to the preliminary test, the mass ratio of biochar to pyrite was set at 3:1, which was the ratio of the best degradation performance. Then, the ground mixture (FeS_2+BC) was calcined at 600 ℃ for 2 h in a nitrogen atmosphere. The final product after calcination was named as FeS_2/BC.

The surface morphology and structure of FeS_2, BC and FeS_2/BC were observed by scanning electron microscopy (SEM, TESCAN MIRA4, Czech). The element distributions of FeS_2, BC and FeS_2/BC were characterized by an energy dispersion spectrometer (EDS) loaded on SEM. The specific surface area, pore volume and pore

size distribution of BC and FeS_2/BC were measured by the automated gas sorption analyzer (Quantachrome AUTOSORB IQ, USA), the material samples used for characterization were all passed through a 100-mesh sifter to maintain similar particle size. The surface functional groups of the catalysts were identified by Fourier transform infrared spectrometer (FTIR, Bruker VERTEX 70 & ALPHA, Germany). The phase structure of materials was characterized by X-ray diffractometer (XRD, Bruker D8 Advance, Germany). Valence states of elements on the surface of FeS_2/BC before and after reaction were identified by X-ray photoelectron spectrometer (XPS, Thermo Scientific K-Alpha, USA). Zeta potential was measured by Zetasizer (Malvern Zetasizer Nano ZS90, UK). Linear sweep voltammetry (LSV) was carried out by electrochemical workstation (CHI 760E, China), proceeding in a three-electrode system. Electrochemical Information: The FeS_2/BC was loaded on a glassy carbon electrode as the working electrode. Pt electrode and Ag/AgCl electrode were used for counter electrode and reference electrode respectively. 0.2 M Na_2SO_4 solution (pH=3.0) was used as electrolyte solution.

2.3. Experimental method

All degradation experiments were performed at conical flasks (250 mL) with magnetic agitation at room temperature, and the solution volume was 100 mL. The FeS_2/BC and H_2O_2 were put into the CIP solution at the same time to initiate the reaction. Unless otherwise stated, the conventional reaction conditions were set as: the initial concentrations of CIP, FeS_2/BC and H_2O_2 were 30 mg/L, 1.5 g/L and 5 mM,

169 respectively. The initial concentration of CIP in the total organic carbon (TOC)
170 experiment was the same as above, which was also 30 mg/L. The initial pH of CIP
171 solution was 3.0, and the reaction lasted for 20 min. One milliliter solution was sampled
172 at each predetermined time. The sample was filtered by a nylon filter membrane of 0.45
173 μm, and 20 μL of tert-butanol (TBA) were added as a quenching agent. All the
174 experiments were performed in triplicate.

175 To ascertain the optimum reaction conditions for the CIP degradation by
176 heterogeneous Fenton reaction catalyzed with FeS_2/BC, a series of experiments were
177 proceeded under various FeS_2/BC dosage (0.5–3.0 g/L), H_2O_2 dosage (1–20 mM) and
178 initial pH of solution (3–9). To comparatively examine the performance of different
179 systems for CIP degradation, the total amount of catalyst in each system was controlled
180 at 1.5 g/L.

181 2.4. Analytical method

182 The high-performance liquid chromatography system (HPLC) (Agilent 1100,
183 USA) was used to determine the concentration of CIP which equipped with a C18
184 column. The mobile phase was comprised of methanol and 0.1% formic acid (Liu et al.,
185 2017b; Liu et al., 2021). The intermediates that might exist in the degradation process
186 were detected by ultrahigh-performance liquid chromatography system (UPLC)
187 (Agilent 1290, USA) in tandem with mass spectrometry system (MS) (Agilent QTOF
188 6550, USA) (Details is provided in Text S1). TOC was analyzed by TOC analyzer
189 (TOC-V, Shimadzu, Japan). The concentrations of Fe(II) and total Fe in solution was

detected by 1,10-phenanthroline spectrophotometry at 510 nm (Zhu et al., 2020). The free radicals generated from the Fenton system catalyzed by FeS_2/BC were identified by electron spin resonance (ESR, Bruker A300, Germany).

3. Results and discussion

3.1. Characterization of catalysts

SEM images of catalysts are displayed in Fig. 1. The BC presented a loose and porous structure, and the shape of FeS_2 was fragments or particles. As can be seen from Fig. 1c, FeS_2 was observed on the surface of biochar, and the preparation process of FeS_2/BC made the surface of biochar rougher. The corresponding EDS spectra showed the composition of surface elements, and the existence of Fe and S peak (Fig. S1(c)) further proved the successful loading of pyrite. The element mass fraction of different materials was presented in Table S1, Fe accounted for 15.59 wt% in FeS_2/BC, which basically accorded with the coupling ratio. Given by Table S2, the specific surface area of FeS_2/BC was 15.076 m^2/g, which was nearly 3 times that of BC. The pore volume also got promoted from 0.026 to 0.037 cm^3/g. According to studies of Pan et al. (2021) and Tang et al. (2021), grinding of biochar and calcination at higher temperature contribute to the increase of specific surface area and pore volume, which was consistent with our experimental results. The increase of these parameters was helpful to the adsorption of ciprofloxacin during degradation. As shown in Fig. S2, most of the pores of BC and FeS_2/BC were 3–9 nm mesopores, and the existence of H3 hysteresis

loop also proved the mesoporous structure (Thommes et al., 2015).

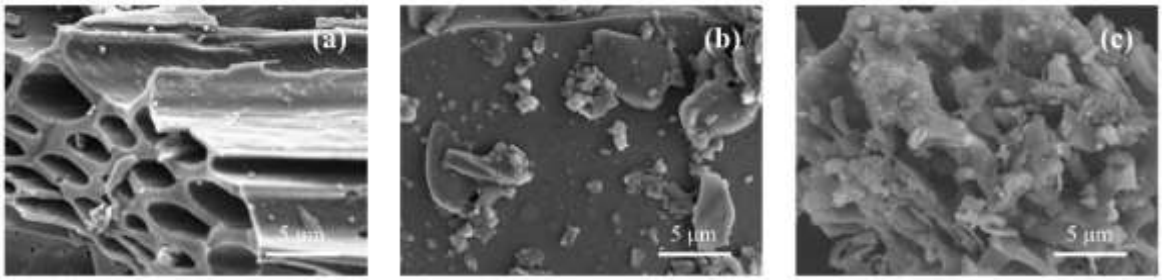

Fig. 1. SEM images of BC (a), FeS_2 (b) and FeS_2/BC (c).

FTIR was adopted to ascertain main functional groups, and the results of different materials were shown in Fig. 2 (clear picture around 400 cm^{-1} wavenumber can be seen in Fig. S3). For BC, the stretching vibration of –OH, C=C/C=O, C–O, C–H, and Si–O could be confirmed by the peaks at 3385, 1580, 1093, 795 and 456 cm^{-1}, respectively (Yang et al., 2019). For FeS_2, the peak at 1080 cm^{-1} matched the stretching vibration of S=S (Tang et al., 2021). The peak at 417 cm^{-1} was acknowledged as one of the peaks in the standard FTIR spectrum of pyrite (Sun et al., 2017). Compared with BC, the peaks at –OH and C=C/C=O of FeS_2/BC were decreased, and the peaks at 1080–1093 cm^{-1} was enhanced, which might be caused by the superposition of the stretching vibration effects of C–O and S=S. However, no peak indicating FeS_2 was found at about 417 cm^{-1} of the FeS_2/BC spectrum. This might be due to the high content of biochar in the FeS_2/BC (the mass ratio of biochar to pyrite was 3:1) and its smaller density than that of pyrite, and thus the volume ratio of biochar in the FeS_2/BC was much larger than that of pyrite, resulting in masking of the characteristic peaks of pyrite. To further determine whether the pyrite had changed during calcination, XRD analysis of the catalysts were performed (results are shown in Fig. S4). It can be seen that the

peak of FeS_2/BC was almost the same as the peak type of biochar, and no peak related to iron was detected, which was consistent with the masked situation in the FTIR spectra. We calcined pyrite with the same procedure of synthesizing FeS_2/BC. The peaks of calcined FeS_2 at 28.5°, 33.1°, 37.1°, 40.8°, 47.4°, 56.3°, 59.0°, 61.7°, 64.3°, 76.6° and 78.9° were assigned to (111), (200), (210), (211), (220), (311), (222), (023), (321), (331) and (420) FeS_2 (PDF# 42–1340) (Nie et al., 2022), which was consistent with the original pyrite and proved that the calcination does not change the phase structure of pyrite.

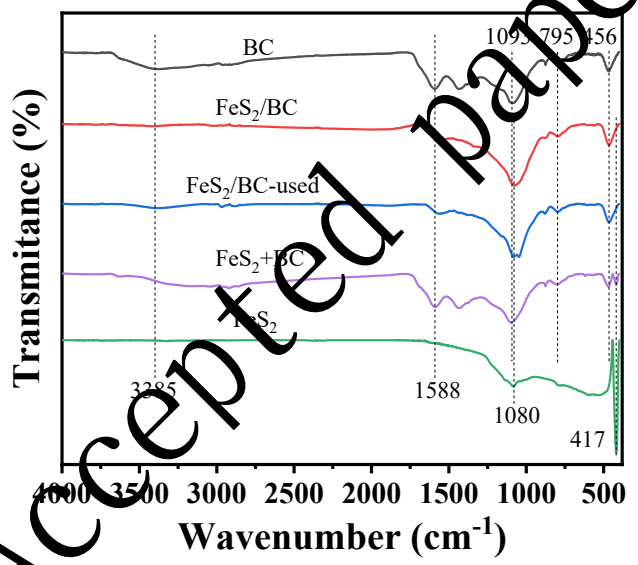

Fig. 2. FTIR spectra of BC, FeS_2/BC, FeS_2/BC after reaction, FeS_2+BC and FeS_2.

Fig. 3 depicts the XPS results of FeS_2 and FeS_2/BC. Fig. 3a gives the Fe 2p spectrum of FeS_2. The peaks at 707.1 and 719.8 eV should be attributed to Fe(II)–S in pyrite (Du et al., 2020; Nie et al., 2022), while the peaks around 710.7 eV were due to Fe^{3+} states from oxidation of the pyrite surface (Wang et al., 2021). The Fe 2p spectrum of FeS_2/BC is given in Fig. 3b. There were double peaks of Fe(II) and Fe(III), and it was in line with the study of Yang et al. (2019), who also calcined pyrite. The presence

of S_2^{2-} and S_n^{2-} could be confirmed by the peaks at 162.6 and 163.9 eV, respectively (Du et al., 2020). The peaks at 168.7 and 169.8 eV corresponded to SO_4^{2-}, which could be derived from alkaline-earth sulfates existed in pyrite (Wang et al., 2021). For FeS_2/BC before and after reaction, the peaks of S_2^{2-} and S_n^{2-} were basically consistent with those of pyrite, which suggested that the structure of pyrite was hardly changed.

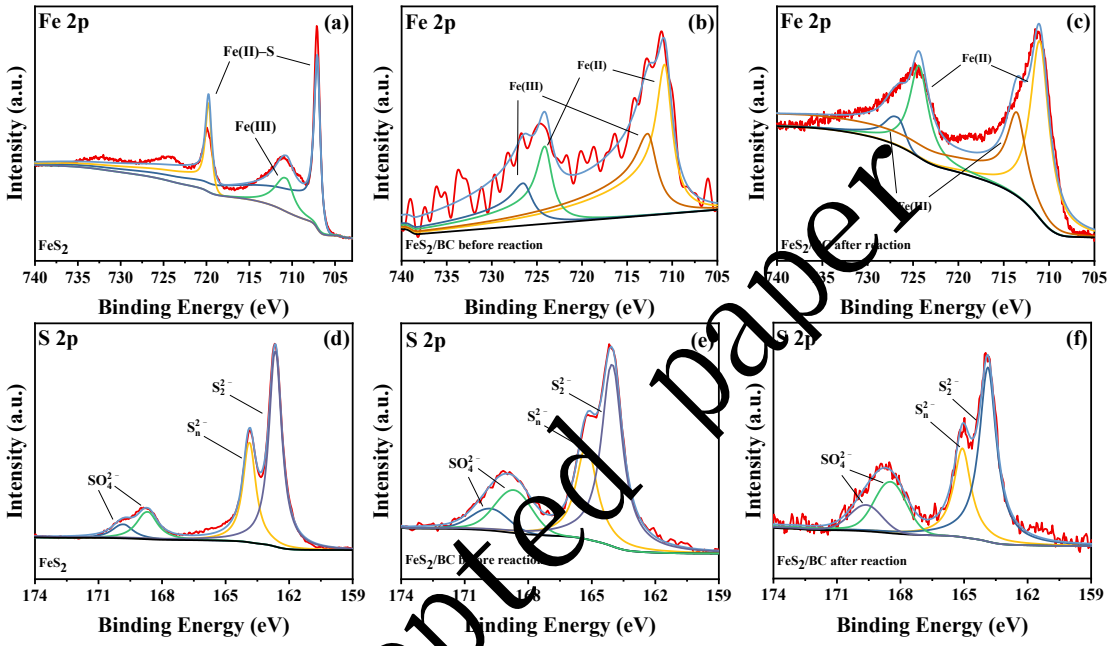

Fig. 3. XPS spectra of FeS_2 (a and d), FeS_2/BC before (b and e) and after (c and f) reaction.

3.2. Comparison of CIP removal in various systems

The performance of various systems on CIP removal in 20 min are shown in Fig. 4a, and the total amount of catalyst in all systems was 1.5 g/L. When BC was added alone, the removal rate of CIP was 30%, depending on the adsorption capacity of BC. When adding H_2O_2, the removal rate was almost unchanged, indicating the poor ability of BC to activate H_2O_2. The removal rate was 48.6% when FeS_2/BC was added alone, which could take credit to the attack of •OH and $SO_4^{\bullet-}$ generated during reaction (the

reaction mechanism was detailed in section 3.5) and the adsorption capacity enhanced by the increased specific surface area (Yang et al., 2019). The degradation rate of CIP by Fenton system catalyzed by FeS_2 was 83.2%, while that by the Fenton system catalyzed by FeS_2/BC reached 96.8%. The above data showed that compared with other systems, the degradation rate of the FeS_2/BC was greatly improved, which proved the success of the coupling. The catalyst used in FeS_2+BC+H_2O_2 system was a grinding mixture of BC (1.125 g/L) and FeS_2 (0.375 g/L), and its degradation rate of only 41.3%. This group was similar to the study by Zhu et al. (2020), which fully proves that the idea of combining biochar with natural pyrite as a composite material for Fenton degradation was correct and effective. Grinding and calcination made biochar and pyrite closely bound, which may be more conducive to adsorption and degradation. For a more intuitive observation of the rate, the pseudo-first-order model (Eq. (1)) was used for kinetic analysis.

$$\ln(C_0/C_t) = kt \quad (1)$$

where t is the reaction time, and C_0 and C_t are the concentrations of CIP at times 0 and t min, respectively. k represents the rate constant of pseudo-first-order. The rate constant (k) of the FeS_2/BC+H_2O_2 system was 0.357 min^{-1}, which was absolutely superior to BC+ H_2O_2 (0.037 min^{-1}), FeS_2+BC+ H_2O_2 (0.058 min^{-1}) and FeS_2 +H_2O_2 (0.191 min^{-1}) systems (Fig. S5). This proved that the Fenton system catalyzed by FeS_2/BC can degrade CIP effectively and rapidly.

Fig. 4b shows the TOC removal efficiency in different systems, which indicates

the complete mineralization of CIP. Obviously, the removal rates of TOC in the $FeS_2+H_2O_2$ and BC+ H_2O_2 systems was very low (<10%). According to the degradation rate of CIP in $FeS_2+H_2O_2$ system (83.2%), it could be speculated that only the molecular structure of CIP was broken, which might be attributed to the less •OH production by pyrite alone. The removal rate was improved in FeS_2/BC and FeS_2+BC+H_2O_2 systems, and it reached a maximum in FeS_2/BC+H_2O_2 system (nearly 45%), which was nearly 5 times that of $FeS_2+H_2O_2$ and BC+ H_2O_2 systems. It indicated that the synergistic effect of biochar and pyrite can produce more free radicals, and the attack effect on pollutants was stronger. In conclusion, the Fenton system catalyzed by FeS_2/BC showed the best performance. Although the TOC removal rate was not too high, the time required was short (only 20 min) and there was no toxic leaching. Considering that the original concentration of TOC was 30 mg/L, the actual degradation effect reached nearly 13.5 mg/L, which still showed a good application value compared with previous studies (Luo et al., 2019; Wang and Zhuan, 2020).

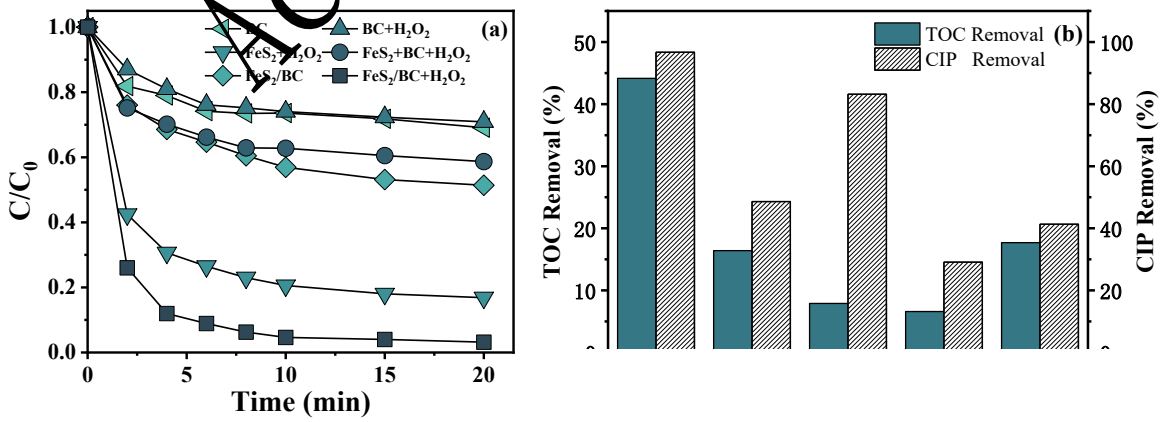

Fig. 4. Removal of CIP (a) and TOC (b) in various systems. Reaction conditions: $[CIP]_0$ = 30 mg/L, $[catalyst]_0$ = 1.5 g/L, $[H_2O_2]_0$ = 5 mM, and initial pH = 3.

3.3. Effect of FeS_2/BC dosage, H_2O_2 concentration, different anions and reusability on the CIP degradation

As the dosage of FeS_2/BC increased from 0.5 to 1.5 g/L, the degradation efficiency increased from 83.7% to 96.8%, and k also increased from 0.1937 to 0.357 min^{-1}. However, when dosage came to 2.0 and 3.0 g/L, the efficiency decreased to 75.7% (k = 0.1541 min^{-1}) and 52.0% (k = 0.0891 min^{-1}), respectively (Fig. 5a). Fenton reaction takes •OH as the main free radical to degrade pollutants (Eq. (2)). This might be due to the excessive amount of Fe^{2+} brought by excessive catalyst, leading to the scavenging reaction between Fe^{2+} and free radicals (Eq. (3)), which was consistent with the results of others (Zhang et al., 2014). Therefore, the best dosage of catalyst was determined to be 1.5g/L. Depicted in Fig. 5b, as the concentration of H_2O_2 increased from 1 to 5 mM, the efficiency increased and the degradation of CIP was accelerated. The corresponding k increased from 0.1231 to 0.357 min^{-1}. As it came to 10 and 20 mM, the degradation rate decreased slightly and k also dropped to 0.3301 and 0.2684 min^{-1}, according to the study of Xue et al. (2009), it could be interpreted as the consumption of active free radicals by high concentration of H_2O_2 (Eq. (4)). Therefore, both in terms of cost and degradation efficiency, the best concentration of H_2O_2 was determined to be 5 mM.

The quality of real wastewater is complex. Considering the practical application, the effect of common anions in water such as Cl^- (Li et al., 2022), NO_3^- (Bergquist et al., 2016), HCO_3^- (Santafé-Moros and Gozálvez-Zafrilla, 2010) and SO_4^{2-} (Ao et al., 2020) on the CIP degradation was investigated. The anion was added to the CIP

318 solution before the reaction at the same concentration as the H_2O_2, which was 5 mM.
319 In Fig. 5c, it was obviously that Cl^-, NO_3^- and SO_4^{2-} displayed little restriction on the
320 degradation efficiency of CIP, demonstrating that the Fenton system catalyzed by
321 FeS_2/BC had good applicability for treating wastewater containing various anions. It
322 was known that Cl^- could quench •OH (Eq. (5)), whereas only a slight effect was
323 exerted on this system, which could be explained as the generated Cl• still had
324 relatively good reactivity ($E^0[Cl•/Cl^-]$ =2.55 V) to achieve the degradation of CIP, and
325 the result was consistent with the study of Nie et al. (2022). However, the presence of
326 HCO_3^- had a great inhibiting effect on degradation, which could be attributed to two
327 aspects. One was the consumption of H^+ by HCO_3^- in the solution (Patra et al., 2020).
328 As a result of this, Fe(II) was difficult to be released from FeS_2/BC. The other was that
329 •OH reacted with HCO_3^- to generate $CO_3^{•-}$ with weak oxidizing ability (Eq. (6)), which
330 hindered degradation of CIP (Luo et al., 2020). In the actual Fenton process, the pH is
331 generally adjusted to 2.5-3.5 in advance (Yuan et al., 2019), during which the HCO_3^-
332 in solution can be removed, so the influence of this ion is limited.

333 On the basis that the dosage of the first catalyst was 1.5 g/L and no additional
334 catalyst was added, the reuse experiment was carried out. At the end of each reaction,
335 the catalyst was filtered through filter paper and washed briefly before being put into
336 the next experiment. The degradation rate of CIP of the 2nd, 3rd, and 4th cycles decreased
337 to 84%, 74% and 57%, respectively (Fig. 5d). The relatively high degradation rate was
338 maintained in the second cycle, because the less loss of active components such as iron

and sulfur species, which was consistent with the results of FTIR (Fig. 2) and XPS (Fig. 3c and 3f). The degradation rate decreased significantly in the fourth cycle, which may be due to more loss of iron and sulfur species caused by multiple cycles, loss during catalyst recovery, and the blocking of the active sites by residual intermediates (Li et al., 2021).

$$Fe^{2+}+H_2O_2+H^+\rightarrow Fe^{3+}+\bullet OH+H_2O \quad (2)$$

$$Fe^{2+}+\bullet OH\rightarrow Fe^{3+}+OH^- \quad (3)$$

$$H_2O_2+\bullet OH\rightarrow HO_2\bullet+H_2O \quad (4)$$

$$\bullet OH+Cl^-\rightarrow ClOH^{\bullet-}\rightarrow Cl\bullet+OH^- \quad (5)$$

$$\bullet OH+HCO_3^-\rightarrow CO_3^{\bullet-}+H_2O \quad (6)$$

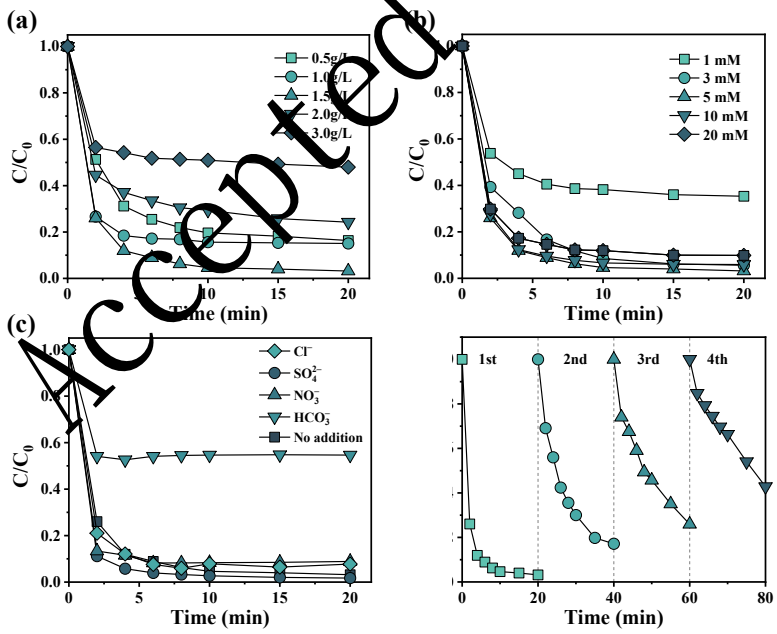

Fig. 5. Effect of catalyst dosage (a), H_2O_2 concentration (b), different anions (c) and reusability on the degradation of CIP in the Fenton system catalyzed by FeS_2/BC. Reaction conditions: $[CIP]_0$ = 30 mg/L, $[H_2O_2]_0$ = 5 mM, and initial pH = 3.

353 3.4. Study on pH in CIP degradation process

354 The pH of solution is one of the considerable factors affecting Fenton reaction. In
355 Fig. 6a, the degradation rate increased with the decrease of pH and reached the
356 maximum value at pH=3.0, which was in line with most of the Fenton reaction
357 phenomena (Chen et al., 2015; Diao et al., 2017). In order to further ascertain what had
358 happened, the changes of solution pH with the addition of FeS_2/BC under different
359 conditions were studied (Fig. 6b). It could be observed that when FeS_2/BC was added
360 to the water, the pH increased rapidly from 7.0 to about 10.4, proving that FeS_2/BC was
361 alkaline. Known from the literature (Cantrell et al., 2012; Waqas et al., 2018),
362 agricultural waste-derived biochar usually tends to be alkaline, and biochar accounted
363 for a large proportion of the FeS_2/BC (Mass ratio of BC:FeS_2=3:1), which explained
364 the alkalinity of FeS_2/BC. When the initial pH of FeS_2/BC catalyzed Fenton system was
365 3.0, the solution pH rose to about 4.5, which not only achieved excellent degradation
366 rate, but also reduced the consumption of subsequent neutralizing acidic solution (Yuan
367 et al., 2019).

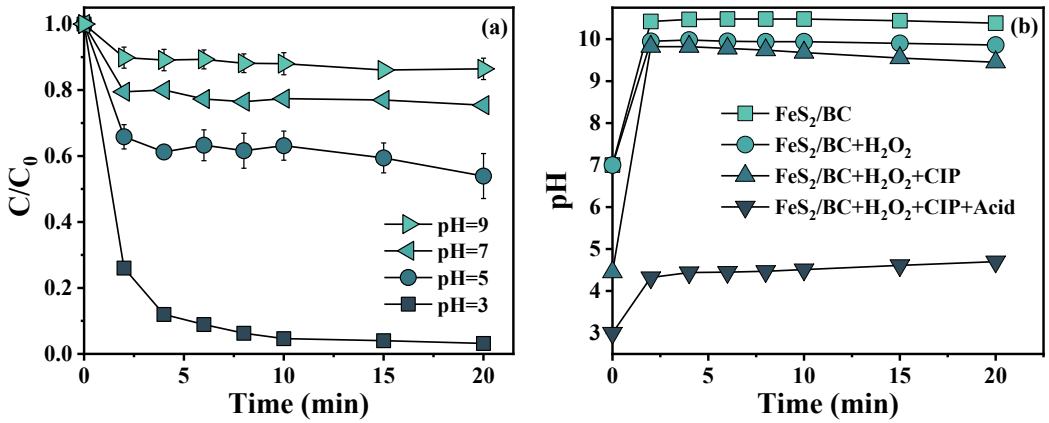

368

369 **Fig. 6.** Study on initial pH of solution on the degradation of CIP in the Fenton system catalyzed

by FeS_2/BC (a) and changes of pH in different systems (b). Reaction conditions: $[CIP]_0$ = 30 mg/L, $[catalyst]_0$ = 1.5 g/L, $[H_2O_2]_0$ = 5 mM.

3.5. Reaction mechanisms

The main reaction of the change of Fe concentration in aqueous solution is shown in the Eq. (2) and Eqs. (7)–(9). When the FeS_2/BC catalyst was added to the CIP solution, Fe(II) was released, and then the Fenton reaction occurred to generate Fe(III), and Fe(II) was consumed. The concentration of aqueous Fe(II) rose rapidly at the initial stage of reaction and reached its peak in about 5 min, and then began to decline (Fig. 7). The Fe(II) concentration was still relatively high within 10 min to keep the reaction going. Correspondingly, the degradation rate was the fastest in the first 5 min of the reaction, and the reaction basically reached the end point at 10 min (degradation rate=95.4%) (Fig. 4a). This phenomenon was basically consistent with the study of Zhang et al. (2014) using natural pyrite to catalyze the degradation of pollutants. When it comes to aqueous Fe(III), unlike the continuous growth in classic Fenton, the concentration rose gradually after the reaction began and remained relatively stable. We assumed that there were two reactions existed. On the one hand, according to Eqs. (8) and (9), there was a transition from Fe(III) to Fe(II). On the other hand, given by section 3.4, solution pH increased gradually to about 4.5 during the reaction, and the solubility of Fe decreased correspondingly, which could also be responsible for the decrease of aqueous Fe (especially Fe(III)) (Nie et al., 2022).

Given the FTIR comparison of the FeS_2/BC before and after reaction (Fig. 2), the

peak intensities of C=C/C=O, C–O and C–H decreased slightly, it was speculated that these groups played roles during the reaction process. The decrease in the peak intensity of the Si–O could be explained by providing the adsorption sites for CIP (Yang et al., 2019). Based on XPS results (Fig. 3c and 3f), after reaction, the peak shape of Fe did not change remarkably, and the obvious peak of Fe(II) could still be clearly observed, indicating the stability of the FeS_2/BC. The content ratio of Fe(II)/Fe(III) before and after the reaction was 1.252 and 1.345, respectively. The proportion increased slightly after the reaction, which may be due to the presence of an oxide layer on the surface of the material before the reaction, so that the content of Fe(III) was larger. The zeta potential values of BC and FeS_2/BC at different pH were illustrated in Fig. 7c and 7d. For original biochar, except for the positive charge at pH=2, it was negatively charged under other pH values (3–10), and the synthesized composite FeS_2/BC were always negatively charged when the pH value ranged from 2 to 10, which meant that biochar and the composite FeS_2/BC were negatively charged under conventional reaction conditions (pH=3).

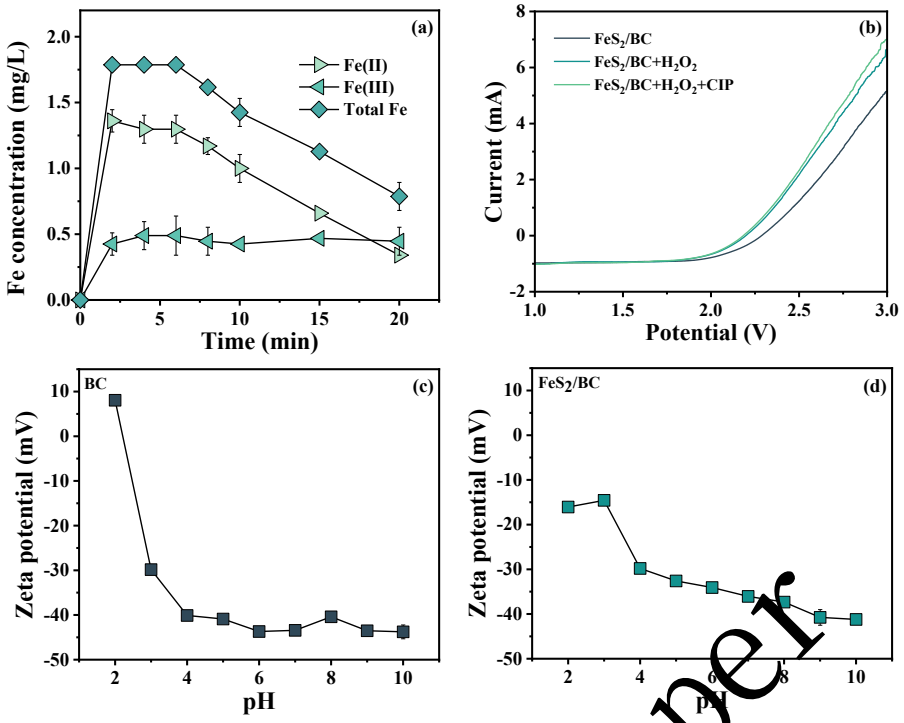

406

407 **Fig. 7.** The changes of Fe(II) and Fe(III) concentrations in the Fenton system catalyzed by

408 FeS_2/BC (a), LSV curves in different reaction systems (no magnetic stirring) (b), and zeta

409 potential values of BC (c)and FeS_2/BC (d) under different pH values. Reaction conditions:

410 $[CIP]_0$ = 30 mg/L, $[catalyst]_0$ = 1.5 g/L, $[H_2O_2]_0$ = 5 mM, and initial pH = 3.

411 For the purpose of determining the active reactive species that existed during the

412 reaction, the quenching experiments were proceeded with tert-butanol (TBA) and

413 chloroform (CF) to quench •OH and $O_2^{\bullet-}$, respectively (Fig. 8a) (Bae et al., 2013; He

414 et al., 2021). When TBA and CF were added before the initiation of reaction, the

415 degradation rates of CIP were observed to drop to 57.2% (k = 0.0769 min^{-1}) and 87.6%

416 (k = 0.1607 min^{-1}), respectively, showing that •OH was the main active species in

417 Fenton reaction. Learned from the study of Yang et al. (2019), $SO_4^{\bullet-}$ might be produced

418 during the reaction due to the presence of pyrite. To further determine the types of free

419 radicals existed, ESR experiments were carried out without adding pollutants. DMPO

was chosen as trapping agent. As presented in Fig. 8b, the characteristic peaks of high intensity corresponding to •OH and low intensity corresponding to $SO_4^{\bullet-}$ could be observed. The intensity of •OH increased with time, while the intensity of $SO_4^{\bullet-}$ increased inconspicuously. In Fig. 8c, the characteristic peak of $O_2^{\bullet-}$ could be observed and the intensity increased with time. Based on the quenching results and ESR spectra, three kinds of free radicals including •OH, $O_2^{\bullet-}$ and $SO_4^{\bullet-}$ were detected in the Fenton system catalyzed by FeS_2/BC, and •OH was the predominant.

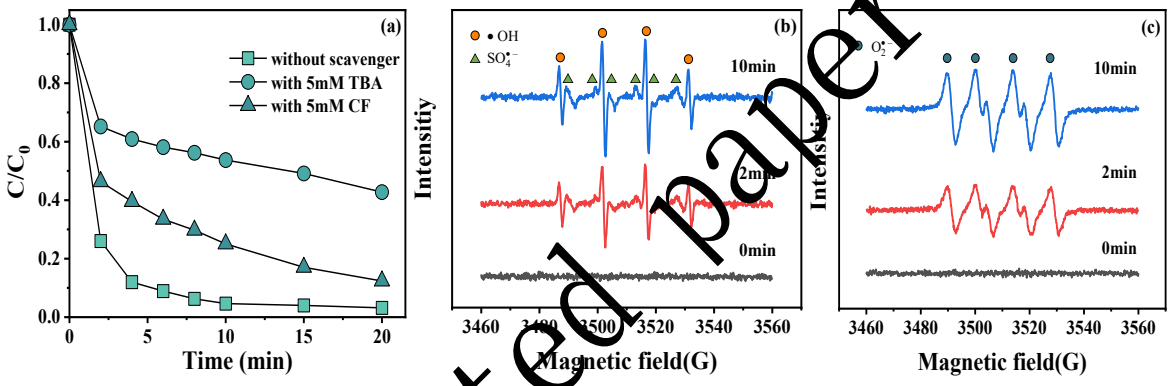

Fig. 8. Effects of different free radical scavengers on the degradation of CIP in the Fenton system catalyzed by FeS_2/BC (a) and ESR spectrum of free radicals generated in the Fenton system catalyzed by FeS_2/BC (b and c). Reaction conditions: $[CIP]_0$ = 30 mg/L, $[catalyst]_0$ = 1.5 g/L, $[H_2O_2]_0$ = 5 mM, and initial pH = 3.

To summary, the involved mechanism of FeS_2/BC catalyzed Fenton system could be divided into two aspects (Fig. 9). The one was adsorbing CIP on the material surface by biochar, and the other was degrading the pollutants adsorbed on the surface by generating free radicals. In the reaction, Fe(II) released from the FeS_2/BC reacted with H_2O_2 to produce a large number of •OH (Eqs. (7) and (2)). Sulfur species in FeS_2/BC such as S_2^{2-} and S_n^{2-} reacted with Fe(III) to reduce it to Fe(II) (Eqs. (8)–(9)) (Zhao et

al., 2017; Zhou et al., 2018; Yang et al., 2019). Due to the electronegativity of biochar (based on zeta potential results), the conversion of Fe(III) to Fe(II) will be promoted as well (Yang et al., 2019), which will generate more •OH to attack pollutants, explaining why the TOC removal rate of the FeS_2/BC was more than 5 times that of pyrite alone. We further characterized this process using electrochemical method. Fig. 7b depicted the LSV curves in different systems. The significant increase of current after the addition of H_2O_2 indicated that there was electron transfer in the solution, whereas the current increased little with the addition of CIP, indicating that most of the electron transfer existed in the reaction between Fe(II) with H_2O_2 to generate free radicals, which could provide another evidence for the conversion of Fe species. Additionally, Fe(II) could also react with dissolved oxygen, and the generated $O_2^{\bullet-}$ continued to react with Fe(III) to produce H_2O_2, which in turn facilitated the generation of •OH (Eqs. (10)–(11)) (Diao et al., 2017). This could also explain that in Fig. 4a, the degradation rate of FeS_2/BC alone was much higher than that of BC alone. The ESR results (Fig. 8b) also demonstrated the continuous generation of •OH. It could be seen from the XPS results that the FeS_2/BC contained a large amount of SO_4^{2-}. When plenty of •OH was generated, it will react with SO_4^{2-} to generate $SO_4^{\bullet-}$ to attack pollutants (Eq. (12)) (Li et al., 2020), according with the existence of $SO_4^{\bullet-}$ in ESR spectrum.

$$2FeS_2+7O_2+2H_2O\rightarrow 2Fe^{2+}+4SO_4^{2-}+4H^+ \quad (7)$$

$$FeS_2+14Fe^{3+}+8H_2O\rightarrow 15Fe^{2+}+2SO_4^{2-}+16H^+ \quad (8)$$

$$8Fe^{3+}+S_2^{2-}+8H_2O\rightarrow 8Fe^{2+}+2SO_4^{2-}+16H^+ \quad (9)$$

459 $Fe^{2+}+O_2 \rightarrow Fe^{3+}+O_2^{\bullet-}$ (10)

460 $Fe^{2+}+O_2^{\bullet-}+2H^+ \rightarrow Fe^{3+}+H_2O_2$ (11)

461 $SO_4^{2-}+\bullet OH \rightarrow SO_4^{\bullet-}+OH^-$ (12)

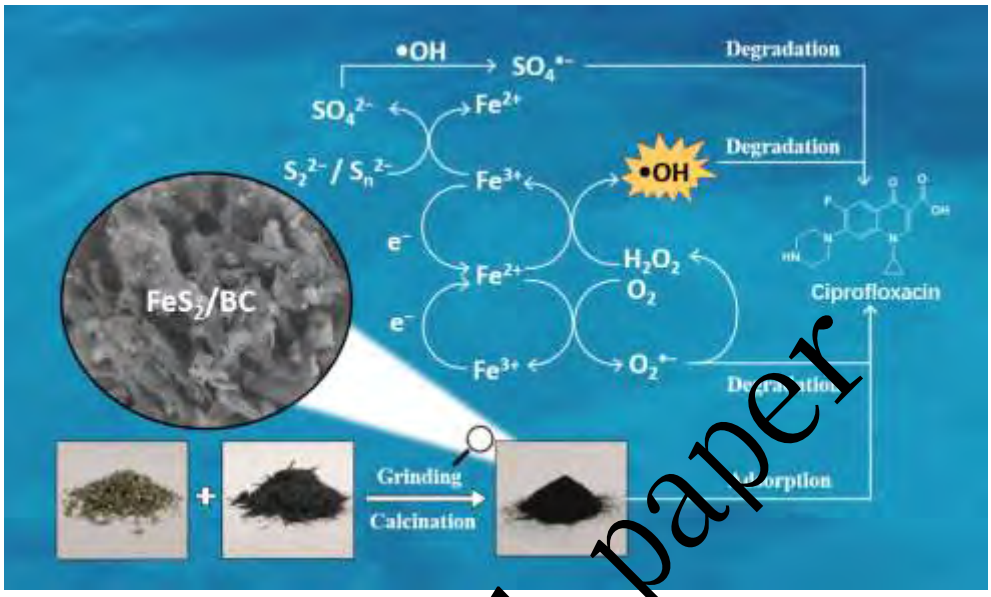

462

463 **Fig. 9.** Reaction mechanisms of CIP degradation in the Fenton system catalyzed by FeS_2/BC.

464 3.6. Intermediates identification and possible degradation pathways

465 During the CIP degradation, the possible intermediates were detected using
466 UPLC-MS. Combining the detected intermediates and previous reports, the cleavage
467 and hydroxylation of the piperazine ring and the substitution or detachment of fluorine
468 might be the prone CIP degradation pathways, and two transformation pathways were
469 proposed (Fig. 10). Pathway I began with hydroxyl substitution on the piperazine ring
470 to form two possible product P1 (m/z 348) and P2 (m/z 348), followed by loss of carbon
471 and oxygen molecules to form P3 (m/z 318) (Chen et al., 2020b). Finally, P3 underwent
472 a decarboxylation reaction to generate P4 (m/z 274). Pathway II also first targeted the
473 piperazine ring. It first underwent a ring-opening reaction to become P5 (m/z 362).

Then, the carbonyl group was removed to form P6 (m/z 334), and the carbonyl group was lost for the second time to produce P7 (m/z 306) (Li et al., 2020). P7 was defluorinated to transform to P8 (m/z 288) under the attack of free radicals. Subsequently, the amine nitrogen was removed to form P9 (m/z 245) through continuous oxidation (Deng et al., 2017). So far, the piperazine ring was thoroughly broken. Finally, the above intermediates could be mineralized to low-molecular-weight products such as carbon dioxide and water through further oxidation and degradation. Information about the above intermediates was given in Table S3.

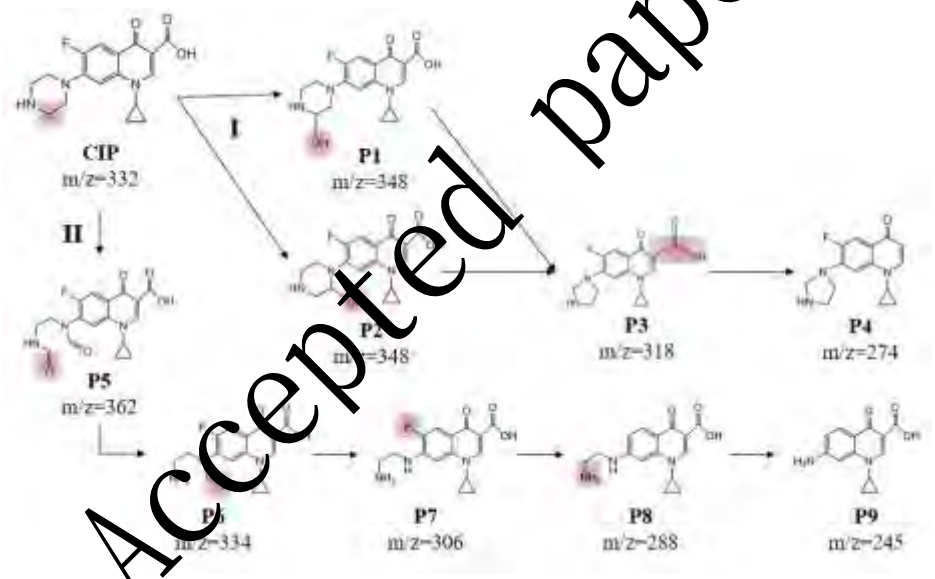

Fig. 10. Possible intermediates and pathways of CIP degradation in Fenton system catalyzed by FeS_2/BC.

3.7. Comparison of performance and cost with previous studies

Table 1 presents a summary of CIP degradation by different Fenton systems. Compared with the previous Fenton process studies, the Fenton system catalyzed by FeS_2/BC in this study is superior to those reported by other studies in terms of initial

concentration, degradation time, and degradation rate. This result indicated that FeS_2/BC was a valuable catalyst to remove organic pollutants in water. Moreover, the preparation of FeS_2/BC required only rice straw derived-biochar and natural pyrite with no additional chemical reagent. Campbell et al. (2018) pointed out that it was more economically viable to use waste biomass feedstocks rather than higher-cost dedicated biomass. On the basis of data showed by The Ministry of Agriculture and Rural Affairs, China produces about 9×10^8 t of straw each year, with about 2×10^8 t unused. This proved that it was economical to use rice straw as raw material. According to the study of Logeswaran et al. (2020), the recycling price of rice straw was less than 18 \$/t. Our previous study showed that the price of natural pyrite was between 100–300 \$/t (Song et al., 2022c). According to the compounding ratio (biochar to pyrite was 3:1), the cost of the raw material was calculated at 38.5–88.5 \$/t. Compared with other catalysts, it could be found that the catalyst provided in this paper FeS_2/BC had better degradation effect at lower cost than most catalysts. Hence, FeS_2/BC could be considered as an effective catalyst with low economic cost.

505 **Table 1**

506 Comparison of performance and cost with other studies for Fenton degradation of CIP.

Catalyst	C_0	Reaction time	Degradation rate	Material cost	References
FeS_2/BC	30 mg/L	20 min	96.8%	38.5–88.5 $/t	This work
HNO_3 modified sludge biochar	10 mg/L	24 h	93%	60 $/t [a]	Luo et al. (2019)
Fe(III) grafted $BiVO_4$+Vis	10 mg/L	120 min	Nearly 50%	About 21.7 $/kg [b]	Gao et al. (2019)
GLDA/Fe(III)	10 mg/L	180 min	96.5%	1.2 $/kg [c]	Ren et al. (2021)
Ball-milled Fe_3O_4 nanoparticle	10 mg/L	120 min	88.9%	9.49 $/kg [d]	Hassani et al. (2018)
(-FeOOH)/MWCNTs nanocomposite	10 mg/L	136 min	86.9%	600–800 $/kg [e]	Salari et al. (2021)

507 [a] This is the price of sewage sludge according to the report by Wzorek and Tańczuk (2015).

508 [b] This is the price of NH_4VO_3 (raw materials of $BiVO_4$) according to the report by Zhang et al.

509 (2022).

510 [c] This is the price of GLDA according to the report by Wang et al. (2022).

511 [d] This is the price of Fe_3O_4 nanoparticles according to the report by Cho et al. (2015).

512 [e] This is the price of MWCNTs according to the report by Liu et al. (2017a)

513 **4. Conclusions**

514 In this paper, two low-cost materials, rice straw biochar and natural pyrite, were
515 ground and calcined to synthesize catalyst for heterogeneous Fenton treatment. The
516 physical and chemical properties of FeS_2/BC were characterized. Through a series of
517 experiments, it was found that the Fenton system catalyzed by FeS_2/BC could degrade

CIP by 96.8% within 20 min under the optimum conditions, and the TOC removal rate was more than 5 times that of the pyrite or biochar catalyzed Fenton system. The degradation effect of FeS_2/BC was much better than the grinding mixture of biochar and pyrite, indicating the effectiveness of the calcination step in the synthetic process. The FeS_2/BC was alkaline in water, and the pH of the solution after Fenton reaction was about 4.5, reducing the cost of subsequent neutralization. No sludge visible to the naked eye was observed after the Fenton reaction catalyzed by FeS_2/BC. The reaction mechanism of CIP degradation by FeS_2/BC was proposed. Rice straw biochar and natural pyrite complemented each other. Both biochar and S(-II) promoted the conversion of Fe species. Based on quenching experiment and ESR spectra, there were three kinds of free radicals (•OH, $O_2^{\bullet-}$ and $SO_4^{\bullet-}$) in the Fenton system and •OH was the main radicals for degrading CIP. With the aid of mass spectrometry analysis, two degradation pathways of CIP were proposed. Compared with other studies, the FeS_2/BC has certain merits in terms of performance and cost. In summary, the synthesized FeS_2/BC provides an idea for solid waste treatment and has good scientific and practical value in the treatment of antibiotic wastewater. In summary, the synthesized FeS_2/BC provides a novel idea for both solid waste treatment and pollution elimination, and has good scientific and practical value for the treatment of antibiotic wastewater.

Acknowledgements

This work was supported by the National Natural Science Foundation of China (U20A20323, 52100180, 51521006, 52170162), the Fundamental Research Funds for

539 the Central Universities (531118010817), the China National Postdoctoral Program for
540 Innovative Talents (BX20200119), the Project funded by China Postdoctoral Science
541 Foundation (2021M690961), and the Hunan Provincial Natural Science Foundation of
542 China (2021JJ40087).

543

References

Ao, H., Cao, W., Hong, Y., Wu, J. and Wei, L. 2020. Adsorption of sulfate ion from water by zirconium oxide-modified biochar derived from pomelo peel. Sci. Total. Environ. 708, 135092.

Bae, S., Kim, D. and Lee, W. 2013. Degradation of diclofenac by pyrite catalyzed Fenton oxidation. Appl. Catal. B: Environ. 134-135, 93-102.

Bergquist, A.M., Choe, J.K., Strathmann, T.J. and Werth, C.J. 2016. Evaluation of a hybrid ion exchange-catalyst treatment technology for nitrate removal from drinking water. Water. Res. 96, 177-187.

Campbell, R.M., Anderson, N.M., Daugaard, D.E. and Naughton, H.T. 2018. Financial viability of biofuel and biochar production from forest biomass in the face of market price volatility and uncertainty. Appl. Energ. 230, 330-343.

Cantrell, K.B., Hunt, P.G., Uchimiya, M., Novak, J.M. and Ro, K.S. 2012. Impact of pyrolysis temperature and manure source on physicochemical characteristics of biochar. Bioresource. Technol. 107, 419-428.

Chen, H., Zhang, Z., Yang, Z., Yang, Q., Li, B. and Bai, Z. 2015. Heterogeneous fenton-like catalytic degradation of 2,4-dichlorophenoxyacetic acid in water with FeS. Chem. Eng. J. 273, 481-489.

Chen, L., Li, H., Liu, T., Cui, Y., Li, Y. and Yang, Z. 2020a. Distribution, residue level, sources, and phase partition of antibiotics in surface sediments from the inland river: a case study of the Xiangjiang River, south-central China. Environ. Sci. Pollut. R. 27 (2), 2273-2286.

Chen, S., Huang, D., Zeng, G., Xue, W., Lei, L., Xu, P., Deng, R., Li, J. and Cheng, M. 2020b. In-situ synthesis of facet-dependent BiVO4/Ag3PO4/PANI photocatalyst with enhanced visible-light-induced photocatalytic degradation performance: Synergism of interfacial coupling and hole-transfer. Chem. Eng. J. 382, 122840.

Cho, D.-W., Song, H., Schwartz, F.W., Kim, B. and Jeon, B.-H. 2015. The role of magnetite nanoparticles in the reduction of nitrate in groundwater by zero-valent

572 iron. Chemosphere. 125, 41-49.
573 Deng, J., Dong, H., Zhang, C., Jiang, Z., Cheng, Y., Hou, K., Zhang, L. and Fan, C.
574 2018. Nanoscale zero-valent iron/biochar composite as an activator for Fenton-
575 like removal of sulfamethazine. Sep. Purif. Technol. 202, 130-137.
576 Deng, J., Ge, Y., Tan, C., Wang, H., Li, Q., Zhou, S. and Zhang, K. 2017. Degradation
577 of ciprofloxacin using α-MnO2 activated peroxymonosulfate process: Effect of
578 water constituents, degradation intermediates and toxicity evaluation. Chem. Eng.
579 J. 330, 1390-1400.
580 Diao, Z.H., Xu, X.R., Jiang, D., Li, G., Liu, J.J., Kong, L.J. and Zuo, L.Z. 2017.
581 Enhanced catalytic degradation of ciprofloxacin with FeS2/SiO2 microspheres as
582 heterogeneous Fenton catalyst: Kinetics, reaction pathways and mechanism. J.
583 Hazard. Mater. 327, 108-115.
584 Dong, C.D., Chen, C.W. and Hung, C.M. 2017. Synthesis of magnetic biochar from
585 bamboo biomass to activate persulfate for the removal of polycyclic aromatic
586 hydrocarbons in marine sediments. Bioresource. Technol. 245 (Pt A), 188-195.
587 Du, H., Yang, C., Pu, W., Zeng, L. and Gong, J. 2020. Enhanced Electrochemical
588 Reduction of N2 to Ammonia over Pyrite FeS2 with Excellent Selectivity. ACS.
589 Sustain. Chem. Eng. 8 (28), 10572-10580.
590 Gao, X., Ma, C., Liu, Y., Ying, L. and Yan, Y. 2019. Self-induced Fenton reaction
591 constructed by Fe(III) grafted BiVO4 nanosheets with improved photocatalytic
592 performance and mechanism insight. Appl. Surf. Sci. 467-468, 673-683.
593 Girardi, C., Greve, J., Lamshöft, M., Fetzer, I., Miltner, A., Schäffer, A. and Kästner,
594 M. 2011. Biodegradation of ciprofloxacin in water and soil and its effects on the
595 microbial communities. J. Hazard. Mater. 198, 22-30.
596 Hanna, N., Sun, P., Sun, Q., Li, X., Yang, X., Ji, X., Zou, H., Ottoson, J., Nilsson, L.E.,
597 Berglund, B., Dyar, O.J., Tamhankar, A.J. and Stålsby Lundborg, C. 2018.
598 Presence of antibiotic residues in various environmental compartments of
599 Shandong province in eastern China: Its potential for resistance development and
600 ecological and human risk. Environ. Int. 114, 131-142.

Hassani, A., Karaca, M., Karaca, S., Khataee, A., Açışlı, Ö. and Yılmaz, B. 2018. Preparation of magnetite nanoparticles by high-energy planetary ball mill and its application for ciprofloxacin degradation through heterogeneous Fenton process. J. Environ. Manage. 211, 53-62.

He, C., Xia, W., Zhou, C., Huang, D., Zhang, C., Song, B., Yang, Y., Li, J., Xu, X., Shang, Y. and Du, L. 2022. Rational design to manganese and oxygen co-doped polymeric carbon nitride for efficient nonradical activation of peroxymonosulfate and the mechanism insight. Chem. Eng. J. 430, 132751.

He, J., Tang, J., Zhang, Z., Wang, L., Liu, Q. and Liu, X. 2021. Magnetic ball-milled FeS@biochar as persulfate activator for degradation of tetracycline. Chem. Eng. J. 404.

Inyang, M.I., Gao, B., Yao, Y., Xue, Y., Zimmerman, A., Mosa, A., Pullammanappallil, P., Ok, Y.S. and Cao, X. 2016. A review of biochar as a low-cost adsorbent for aqueous heavy metal removal. Crit. Rev. Env. Sci. Tec. 46 (4), 406-433.

Khan, S., Chao, C., Waqas, M., Arp, H.P.H. and Zhu, Y.-G. 2013. Sewage Sludge Biochar Influence upon Rice (Oryza sativa L) Yield, Metal Bioaccumulation and Greenhouse Gas Emissions from Acidic Paddy Soil. Environ. Sci. Technol. 47 (15), 8624-8632.

Krasucka, P., Pan, B., Sik Ok, Y., Mohan, D., Sarkar, B. and Oleszczuk, P. 2021. Engineered biochar – A sustainable solution for the removal of antibiotics from water. Chem. Eng. J. 405.

Li, J., Pan, L., Yu, G., Xie, S., Li, C., Lai, D., Li, Z., You, F. and Wang, Y. 2019. The synthesis of heterogeneous Fenton-like catalyst using sewage sludge biochar and its application for ciprofloxacin degradation. Sci. Total. Environ. 654, 1284-1292.

Li, L., Liu, S., Cheng, M., Lai, C., Zeng, G., Qin, L., Liu, X., Li, B., Zhang, W., Yi, Y., Zhang, M., Fu, Y., Li, M. and Long, M. 2021. Improving the Fenton-like catalytic performance of MnOx-Fe3O4/biochar using reducing agents: A comparative study. J. Hazard. Mater. 406, 124333.

Li, T., Wang, X., Chen, Y., Liang, J. and Zhou, L. 2020. Producing OH, SO4− and O2−

630 in heterogeneous Fenton reaction induced by Fe3O4-modified schwertmannite.
631 Chem. Eng. J. 393.
632 Li, Y., Yang, Z., Yang, K., Wei, J., Li, Z., Ma, C., Yang, X., Wang, T., Zeng, G., Yu,
633 G., Yu, Z. and Zhang, C. 2022. Removal of chloride from water and wastewater:
634 Removal mechanisms and recent trends. Sci. Total. Environ. 821, 153174.
635 Liu, H., Ren, M., Qu, J., Feng, Y., Song, X., Zhang, Q., Cong, Q. and Yuan, X. 2017a.
636 A cost-effective method for recycling carbon and metals in plants: synthesizing
637 nanomaterials. Environ. Sci. Nano. 4 (2), 461-469.
638 Liu, X., Lu, S., Liu, Y., Meng, W. and Zheng, B. 2017b. Adsorption of
639 sulfamethoxazole (SMZ) and ciprofloxacin (CIP) by humic acid (HA):
640 characteristics and mechanism. RSC Adv. 7 (80), 50449-50458.
641 Liu, Y., Xu, J. and Chen, M. 2021. Synthesis of direct Z-Scheme Bi3NbO7/BiOCl
642 photocatalysts with enhanced activity for CIP degradation and Cr(VI) reduction
643 under visible light irradiation. Sep. Purif. Technol. 276, 119255.
644 Logeswaran, J., Shamsuddin, A.H., Silitonga, A.S. and Mahlia, T.M.I. 2020. Prospect
645 of using rice straw for power generation: a review. Environ. Sci. Pollut. R. 27 (21),
646 25956-25969.
647 Luo, K., Yang, Q., Pang, Y., Wang, D., Li, X., Lei, M. and Huang, Q. 2019. Unveiling
648 the mechanism of biochar-activated hydrogen peroxide on the degradation of
649 ciprofloxacin. Chem. Eng. J. 374, 520-530.
650 Luo, W., Huang, W., Feng, X., Huang, Y., Song, X., Lin, H., Wang, S. and Mailhot, G.
651 2020. The utilization of Fe-doped g-C3N4 in a heterogeneous photo-Fenton-like
652 catalytic system: the effect of different parameters and a system mechanism
653 investigation. RSC Adv. 10 (37), 21876-21886.
654 Lyu, H., Gao, B., He, F., Zimmerman, A.R., Ding, C., Tang, J. and Crittenden, J.C.
655 2018. Experimental and modeling investigations of ball-milled biochar for the
656 removal of aqueous methylene blue. Chem. Eng. J. 335, 110-119.
657 Lyu, H., Tang, J., Cui, M., Gao, B. and Shen, B. 2020. Biochar/iron (BC/Fe) composites
658 for soil and groundwater remediation: Synthesis, applications, and mechanisms.

Chemosphere. 246, 125609.

Michael, I., Rizzo, L., McArdell, C.S., Manaia, C.M., Merlin, C., Schwartz, T., Dagot, C. and Fatta-Kassinos, D. 2013. Urban wastewater treatment plants as hotspots for the release of antibiotics in the environment: A review. Water. Res. 47 (3), 957-995.

Murphy, R. and Strongin, D.R. 2009. Surface reactivity of pyrite and related sulfides. Surf. Sci. Rep. 64 (1), 1-45.

Nguyen, B.T., Chen, Q.L., He, J.Z. and Hu, H.W. 2020. Oxytetracycline and Ciprofloxacin Exposure Altered the Composition of Protistan Consumers in an Agricultural Soil. Environ. Sci. Technol. 54 (15), 9556-9563.

Nie, X., Li, G., Li, S., Luo, Y., Luo, W., Wan, Q. and An, T. 2022. Highly efficient adsorption and catalytic degradation of ciprofloxacin by a novel heterogeneous Fenton catalyst of hexapod-like pyrite nanosheets mineral clusters. Appl. Catal. B: Environ. 300, 120734.

Oberoi, A.S., Jia, Y., Zhang, H., Khanal, S.K. and Lu, H. 2019. Insights into the Fate and Removal of Antibiotics in Engineered Biological Treatment Systems: A Critical Review. Environ. Sci. Technol. 53 (13), 7234-7264.

Pan, X., Gu, Z., Chen, W. and Li, Q. 2021. Preparation of biochar and biochar composites and their application in a Fenton-like process for wastewater decontamination: A review. Sci. Total. Environ. 754, 142104.

Park, J.H., Wang, J.J., Xiao, R., Tafti, N., DeLaune, R.D. and Seo, D.C. 2018. Degradation of Orange G by Fenton-like reaction with Fe-impregnated biochar catalyst. Bioresource. Technol. 249, 368-376.

Patra, S.G., Mizrahi, A. and Meyerstein, D. 2020. The Role of Carbonate in Catalytic Oxidations. Accounts. Chem. Res. 53 (10), 2189-2200.

Premarathna, K.S.D., Rajapaksha, A.U., Sarkar, B., Kwon, E.E., Bhatnagar, A., Ok, Y.S. and Vithanage, M. 2019. Biochar-based engineered composites for sorptive decontamination of water: A review. Chem. Eng. J. 372, 536-550.

Qin, F., Li, J., Zhang, C., Zeng, G., Huang, D., Tan, X., Qin, D. and Tan, H. 2022a.

688 Biochar in the 21st century: A data-driven visualization of collaboration, frontier
689 identification, and future trend. Sci. Total. Environ. 818, 151774.
690 Qin, F., Zhang, C., Zeng, G., Huang, D., Tan, X. and Duan, A. 2022b. Lignocellulosic
691 biomass carbonization for biochar production and characterization of biochar
692 reactivity. Renew. Sust. Energ. Rev. 157, 112056.
693 Qin, Y., Zhang, L. and An, T. 2017. Hydrothermal Carbon-Mediated Fenton-Like
694 Reaction Mechanism in the Degradation of Alachlor: Direct Electron Transfer
695 from Hydrothermal Carbon to Fe(III). Acs. Appl. Mater. Inter. 9 (20), 17115-
696 17124.
697 Ren, H., He, F., Liu, S., Li, T. and Zhou, R. 2021. Enhancing Fenton–like process at
698 neutral pH by Fe(III)–GLDA complexation for the oxidation removal of organic
699 pollutants. J. Hazard. Mater. 416, 126077.
700 Salari, M., Rakhshandehroo, G.R., Nikoo, M.R., Zerafat, M.M. and Mooselu, M.G.
701 2021. Optimal degradation of Ciprofloxacin in a heterogeneous Fenton-like
702 process using (δ-FeOOH)/MWCNTs nanocomposite. Environ. Technol. Inno. 23,
703 101625.
704 Santafé-Moros, A. and Gozálvez-Zafrilla, J.M. 2010. Nanofiltration study of the
705 interaction between bicarbonate and nitrate ions. Desalination. 250 (2), 773-777.
706 Song, B., Almatrafi, E., Sang, F., Wang, W., Zhang, C., Shen, M., Zhou, C., Tang, X.,
707 Zeng, G. and Gong, J. 2022a. Managing Fenton-treated sediment with biochar and
708 sheep manure compost: Effects on the evolutionary characteristics of bacterial
709 community. J. Environ. Manage. 316, 115218.
710 Song, B., Almatrafi, E., Tan, X., Luo, S., Xiong, W., Zhou, C., Qin, M., Liu, Y., Cheng,
711 M., Zeng, G. and Gong, J. 2022b. Biochar-based agricultural soil management:
712 An application-dependent strategy for contributing to carbon neutrality. Renew.
713 Sust. Energ. Rev. 164, 112529.
714 Song, B., Zeng, Z., Almatrafi, E., Shen, M., Xiong, W., Zhou, C., Wang, W., Zeng, G.
715 and Gong, J. 2022c. Pyrite-mediated advanced oxidation processes: Applications,
716 mechanisms, and enhancing strategies. Water. Res. 211, 118048.

717 Sun, Y., Lv, D., Zhou, J., Zhou, X., Lou, Z., Baig, S.A. and Xu, X. 2017. Adsorption
718 of mercury (II) from aqueous solutions using FeS and pyrite: A comparative study.
719 Chemosphere. 185, 452-461.
720 Tang, J., Zhao, B., Lyu, H. and Li, D. 2021. Development of a novel pyrite/biochar
721 composite (BM-FeS2@BC) by ball milling for aqueous Cr(VI) removal and its
722 mechanisms. J. Hazard. Mater. 413, 125415.
723 Thommes, M., Kaneko, K., Neimark, A.V., Olivier, J.P., Rodriguez-Reinoso, F.,
724 Rouquerol, J. and Sing, K.S. 2015. Physisorption of gases, with special reference
725 to the evaluation of surface area and pore size distribution (IUPAC Technical
726 Report). Pure. Appl. Chem. 87 (9-10), 1051-1069.
727 Tian, S., Zhang, C., Huang, D., Wang, R., Zeng, G., Yan, M., Xiong, W., Zhou, C.,
728 Cheng, M., Xue, W., Yang, Y. and Wang, W. 2020. Recent progress in sustainable
729 technologies for adsorptive and reactive removal of sulfonamides. Chem. Eng. J.
730 389, 123423.
731 Van Doorslaer, X., Dewulf, J., Van Langenhove, H. and Demeestere, K. 2014.
732 Fluoroquinolone antibiotics: An emerging class of environmental micropollutants.
733 Sci. Total. Environ. 500-501, 250-269.
734 Varjani, S., Kumar, G. and Rene, E.R. 2019. Developments in biochar application for
735 pesticide remediation: Current knowledge and future research directions. J.
736 Environ. Manage. 232, 505-513.
737 Wang, C., Sun, R., Huang, R. and Cao, Y. 2021. A novel strategy for enhancing
738 heterogeneous Fenton degradation of dye wastewater using natural pyrite:
739 Kinetics and mechanism. Chemosphere. 272, 129883.
740 Wang, H., Guo, W., Yin, R., Du, J., Wu, Q., Luo, H., Liu, B., Sseguya, F. and Ren, N.
741 2019. Biochar-induced Fe(III) reduction for persulfate activation in
742 sulfamethoxazole degradation: Insight into the electron transfer, radical oxidation
743 and degradation pathways. Chem. Eng. J. 362, 561-569.
744 Wang, J. and Tang, J. 2021a. Fe-based Fenton-like catalysts for water treatment:
745 Catalytic mechanisms and applications. J. Mol. Liq. 332.

746 Wang, J. and Tang, J. 2021b. Fe-based Fenton-like catalysts for water treatment:
747 Preparation, characterization and modification. Chemosphere. 276, 130177.
748 Wang, J., Watanabe, N., Inomoto, K., Kamitakahara, M., Nakamura, K., Komai, T. and
749 Tsuchiya, N. 2022. Sustainable process for enhanced CO2 mineralization of
750 calcium silicates using a recyclable chelating agent under alkaline conditions. J.
751 Environ. Chem. Eng. 10 (1), 107055.
752 Wang, J. and Zhuan, R. 2020. Degradation of antibiotics by advanced oxidation
753 processes: An overview. Sci. Total. Environ. 701, 135023.
754 Wang, J.L. and Xu, L.J. 2012. Advanced Oxidation Processes for Wastewater
755 Treatment: Formation of Hydroxyl Radical and Application. Crit. Rev. Env. Sci.
756 Tec. 42 (3), 251-325.
757 Waqas, M., Aburiazaiza, A.S., Miandad, R., Rehan, M., Barakat, M.A. and Nizami,
758 A.S. 2018. Development of biochar as fuel and catalyst in energy recovery
759 technologies. J. Clean. Prod. 188, 477-488.
760 Wzorek, M. and Tańczuk, M. 2015. Production of biosolid fuels from municipal
761 sewage sludge: Technical and economic optimisation. Waste. Manage. Res. 33 (8),
762 704-714.
763 Xue, X., Hanna, K. and Deng, N. 2009. Fenton-like oxidation of Rhodamine B in the
764 presence of two types of iron (II, III) oxide. J. Hazard. Mater. 166 (1), 407-414.
765 Yang, X., Zhang, X., Wang, Z., Li, S., Zhao, J., Liang, G. and Xie, X. 2019.
766 Mechanistic insights into removal of norfloxacin from water using different
767 natural iron ore – biochar composites: more rich free radicals derived from natural
768 pyrite-biochar composites than hematite-biochar composites. Appl. Catal. B:
769 Environ. 255.
770 Yi, Y., Huang, Z., Lu, B., Xian, J., Tsang, E.P., Cheng, W., Fang, J. and Fang, Z. 2020.
771 Magnetic biochar for environmental remediation: A review. Bioresource. Technol.
772 298, 122468.
773 Yuan, D., Zhang, C., Tang, S., Li, X., Tang, J., Rao, Y., Wang, Z. and Zhang, Q. 2019.
774 Enhancing CaO2 fenton-like process by Fe(II)-oxalic acid complexation for

775 organic wastewater treatment. Water. Res. 163, 114861.
776 Zhang, C., Tian, S., Qin, F., Yu, Y., Huang, D., Duan, A., Zhou, C., Yang, Y., Wang,
777 W., Zhou, Y. and Luo, H. 2021. Catalyst-free activation of permanganate under
778 visible light irradiation for sulfamethazine degradation: Experiments and
779 theoretical calculation. Water. Res. 194, 116915.
780 Zhang, W., Li, S.-c., Yan, M., Li, L., Ma, J., Wang, J., Liu, C. and Bao, Y. 2022. In-
781 situ oxidation selective deposition of tetrahedral Ag3PO4{111} on monoclinic
782 BiVO4{040} with highly efficient visible light-driven photocatalysis and long
783 recycling. J. Environ. Chem. Eng. 10 (5), 108418.
784 Zhang, Y., Zhang, K., Dai, C., Zhou, X. and Si, H. 2014. An enhanced Fenton reaction
785 catalyzed by natural heterogeneous pyrite for nitrobenzene degradation in an
786 aqueous solution. Chem. Eng. J. 244, 438-445.
787 Zhao, L., Chen, Y., Liu, Y., Luo, C. and Wu, D. 2017. Enhanced degradation of
788 chloramphenicol at alkaline conditions by S(-II) assisted heterogeneous Fenton-
789 like reactions using pyrite. Chemosphere. 188, 557-566.
790 Zhou, C., Almatrafi, E., Tang, X., Xiao, B., Xia, W., Song, B., Xiong, W., Wang, W.,
791 Guo, H., Chen, S. and Zeng, G. 2022. Investigation on the structure-performance
792 of phthalic acid carboxyl position and carbon nitride towards efficient
793 photocatalytic degradation of organic pollutants. Sep. Purif. Technol. 286, 120464.
794 Zhou, X., Zeng, Z., Zeng, G., Lai, C., Xiao, R., Liu, S., Huang, D., Qin, L., Liu, X., Li,
795 B., Yi, H., Fu, Y., Li, L., Zhang, M. and Wang, Z. 2020. Insight into the
796 mechanism of persulfate activated by bone char: Unraveling the role of functional
797 structure of biochar. Chem. Eng. J. 401.
798 Zhou, Y., Wang, X., Zhu, C., Dionysiou, D.D., Zhao, G., Fang, G. and Zhou, D. 2018.
799 New insight into the mechanism of peroxymonosulfate activation by sulfur-
800 containing minerals: Role of sulfur conversion in sulfate radical generation. Water.
801 Res. 142, 208-216.
802 Zhu, X., Li, J., Xie, B., Feng, D. and Li, Y. 2020. Accelerating effects of biochar for
803 pyrite-catalyzed Fenton-like oxidation of herbicide 2,4-D. Chem. Eng. J. 391.